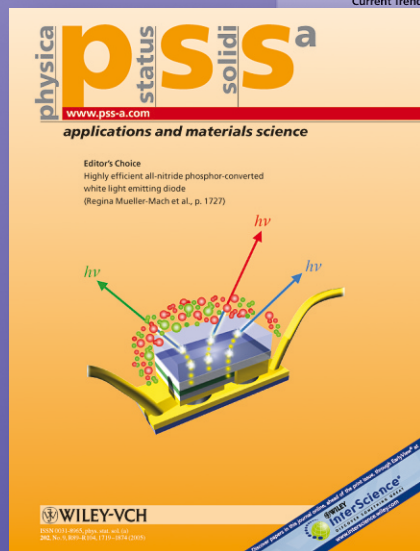


physica p status solidi S S

www.interscience.wiley.com

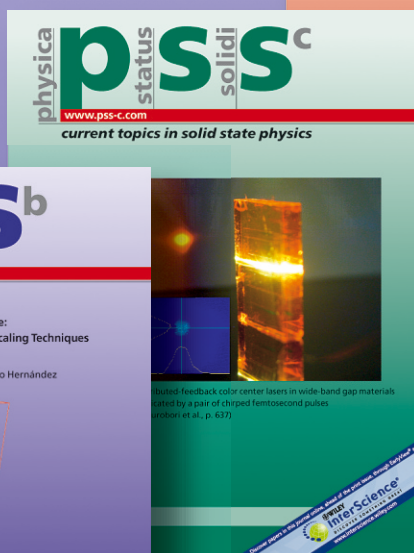
reprints



www.pss-a.com



www.pss-b.com



www.pss-c.com



www.pss-rrl.com

Intensity dependence of quantum efficiency and photo-gating effects in thin film silicon solar cells

Steve Reynolds^{*1}, Charles Main¹, Vladimir Smirnov², and Amjad Meftah³

¹ Carnegie Laboratory of Physics, University of Dundee, Nethergate, Dundee, DD1 4HN, United Kingdom

² IEF-5 Photovoltaik, Forschungszentrum Jülich, Leo Brandt Str., 52425 Jülich, Germany

³ Laboratoire des Matériaux Semiconducteurs et Métalliques, Département de Physique, Université Mohammed Khider, BP145, 07000 Biskra, Algeria

Received 9 August 2009, revised 13 October 2009, accepted 20 October 2009

Published online 18 February 2010

PACS 61.80.Ba, 72.40.Lq, 73.50.Gr, 73.50.Pz, 73.61.Jc, 84.60.Jt

* Corresponding author: e-mail s.z.reynolds@dundee.ac.uk, Phone: +44 (0)1382 384 559, Fax: +44 (0)1382 388 313

Steady-state photoconductivity measurements have been carried out on thin-film silicon pin structures of i-layer thickness typically 4 μm , where crystalline composition has been varied by adjustment of the silane concentration in the process gas. In amorphous and low-crystallinity cells, strongly-absorbed light incident from the p-side at photon fluxes in excess of $10^{14} \text{ cm}^{-2} \text{ s}^{-1}$ produces strongly sub-linear intensity dependence, ‘S’ shaped reverse current-voltage curves and amplification of a second weakly-absorbed beam, termed photogating. These effects are linked to the formation of space charge and attendant low-field region close to the p-i interface, as con-

firmed by computer simulation. More crystalline devices exhibit little or no such behaviour. At lower intensities of strongly-absorbed light there is a markedly steeper increase in reverse current vs. voltage in low-crystalline when compared to amorphous cells, particularly with light incident from the n-side. This suggests the mobility-lifetime product for holes is much larger in the former case, consistent with the higher hole mobilities reported in time of flight studies. Thus the prospect of composition-dependent changes in mobility as well as defect density should be borne in mind when developing materials for application in microcrystalline silicon solar cells.

© 2010 WILEY-VCH Verlag GmbH & Co. KGaA, Weinheim

1 Introduction The electronic properties of silicon thin films vary widely depending on preparation conditions. This is of particular interest in solar cell technology [1], where both amorphous and microcrystalline silicon are used as absorber layers, in single cells or in tandem structures where the complementary nature of their optical bandgaps is used to advantage. Device-quality microcrystalline silicon is a composite material, with optimum solar cells containing a similar proportion of crystalline and amorphous phases controlled by the process gas ratio $SC = [\text{SiH}_4]/([\text{H}_2] + [\text{SiH}_4])$ and monitored by Raman spectroscopy [2] in terms of the crystalline volume fraction I_{CRS} .

Recently, electron and hole transport properties in microcrystalline silicon have been studied using photoconductivity time-of-flight (TOF) measurements [3–5] over a range of I_{CRS} values. It is concluded that, for $I_{CRS} > 30\%$: (i) electron mobility increases by a factor of three, (ii) hole mobility may increase by a factor of over 100, when com-

pared with amorphous silicon. Significant improvement in hole mobility begins at much lower I_{CRS} values, of a few percent. There is also evidence that electron mobility *decreases* from the amorphous value in these low-crystallinity materials [5], which may contribute to the marked decrease in solar cell efficiency in this regime.

Here we report on a range of measurements made under steady-state illumination on the same series of pin structures used in our TOF studies. We hope to discover more about the changes in electronic properties which accompany changes in composition, particularly for low-crystallinity materials which hitherto have not been studied widely, and under conditions more relevant to solar cell operation. One technique we employ is ‘photogating’ [6, 7], in which a photodiode is subject to simultaneous illumination by a strongly-absorbed ‘bias’ beam, and a more weakly absorbed ‘probe’ beam, such that the increase in terminal photocurrent due to the probe beam in the pres-

ence of the bias beam, ΔI_{p+B} , exceeds that due to the probe beam alone, ΔI_p . This may be quantified in terms of a collection efficiency:

$$CE = (\Delta I_{p+B} - \Delta I_p) / qA\phi_p \quad (1)$$

where q is the electronic charge, A the sample area and ϕ_p the probe beam photon flux. We also consider the relationship between photogating and sub-linearity in the flux-ampere relationship, which appears as a characteristic ‘S’ shape in the reverse current - voltage characteristic. [8]. Finally, we consider charge transport under conditions of low optical flux directed from either side of the sample.

2 Experimental Samples were prepared in p-i-n sequence using a cluster-tool system, as described previously [5, 9]. The i-layer, typically 4 μm thick, was deposited by VHF PECVD at 20 W at a rate of typically 0.5 nm/s onto a substrate at 200 °C. Top contacts consisting of 2 mm dots of sputtered ZnO:Al enabled illumination from either side, or from both sides simultaneously. Cells were extensively light-soaked prior to measurement to ensure that their properties remained stable.

Photocurrent measurements were made at room temperature using a Keithley 617 programmable electrometer. Steady photo-excitation, rather than chopped light followed by lock-in detection, was used to accommodate the long settling times characteristic of photogating. High-output LEDs were used as sources at 470 and 640 nm, attenuated as required by means of neutral density filters. Care was taken to exclude extraneous reflected and scattered light by positioning a 1 mm diameter pinhole mask over the contact area.

Computer simulations used in support of this work have been described in previous publications [6, 10]. Here we have used the ‘standard’ defect model, with a spatially-independent Gaussian distribution of deep states. Detailed results will be presented in a future publication.

3 Results and discussion

3.1 Influence of space-charge Figure 1 shows the relationship between photocurrent and photon flux for an amorphous silicon pin sample of thickness 3.9 μm , under short-circuit conditions (0 V) and at 40 V reverse bias. In each case the sample was illuminated through the p-side. An approximately linear curve is obtained under 640 nm (red) illumination in both voltage bias regimes at fluxes up to $10^{16} \text{ cm}^{-2} \text{ s}^{-1}$, with external quantum efficiency limited mostly by optical absorption in the p-layer and by reflection. This indicates complete extraction of photogenerated charge, and no significant build-up of space-charge. Similarly, at 40 V reverse bias under 470 nm (blue) illumination the photoresponse is largely linear. However, under short-circuit conditions the response becomes significantly non-linear above $10^{14} \text{ cm}^{-2} \text{ s}^{-1}$, following an approximately ‘power-law’ relationship. Computer simulations shown in Figure 1 also bear out these trends, which are associated

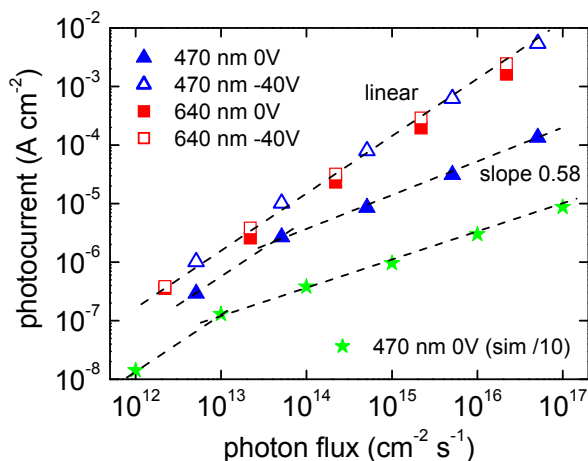


Figure 1 Photocurrent vs. photon flux measured at zero bias and 40 V reverse bias, at wavelengths of 470 and 640 nm, for amorphous silicon pin sample ($SC = 15\%$). A computer simulation is also shown (data scaled down by a factor of 10 for clarity).

with trapped space charge in the vicinity of the p-i interface [10]. This effect has also been investigated as a function of reverse bias voltage at constant flux, as shown in Figure 2. A characteristic ‘S’ shaped current-voltage curve is seen, most prominently at high flux. Simulations reveal that a region of low electric field due to the screening effect of the space charge, limits the electron current that can flow across the i-layer. Increasing reverse bias relieves this ‘bottleneck’, reducing the local recombination rate, and the current increases rapidly. However, unlike a space-charge limited secondary current, where charge can flow in from the contacts, the terminal current in this case cannot exceed the optical generation rate. Thus while the terminal current continues to increase, there is a gradual levelling off until the saturation current is reached. Increased space charge at higher generation rates shifts the curves’ inflection to

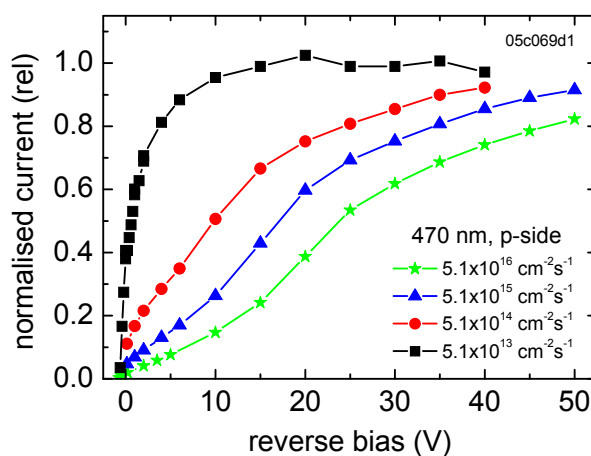


Figure 2 Photocurrent vs. reverse bias voltage for amorphous silicon sample ($SC = 15\%$), over a range of incident flux. Blue light incident from p-side.

progressively higher reverse bias. At low generation rates, the ‘S’ shape is no longer visible and the photocurrent I_p rises steeply with applied reverse bias V_R towards the saturation value I_{Pmax} , broadly following the form:

$$I_p(V) = I_{Pmax} (1 - \exp(-(V_R + V_{BI})/V_0)) \quad (2)$$

where V_{BI} is the built-in p.d. and V_0 is a characteristic voltage, as might be expected if the free electron lifetime remained constant throughout the i-layer. However if the dark current is negligible, recombination will occur predominantly within the generation volume, due to limited supply of thermally-generated holes [8].

3.2 Photogating Figure 3(a) illustrates the photogating effect in the same amorphous silicon sample presented in figures 1 and 2 where the experimental CE is plotted vs. reverse bias. The photogating peak corresponds well to the inflection, the derivative dJ_p/dV having a surprisingly similar shape and peak position. Figure 3(b) shows a computer simulation of these features. Although the agreement is not exact, fine adjustment of the model defect density, capture properties etc. could improve the fit. More importantly, the model correctly predicts the general photogating behaviour and its linkage to modulation of space-charge. Detailed examination reveals that photogating results from holes generated by the probe beam becoming trapped in the bulk of the i-layer, causing a redistribution of the applied field and an increased electron current.

3.3 i-layer composition As SC is decreased the i-layer becomes more crystalline, and a number of changes in the photocurrent vs. reverse bias curves occur. Some representative examples are shown in Figure 4, measured in all cases with 470 nm light incident through the p-layer at a flux of $5.1 \times 10^{16} \text{ cm}^{-2} \text{ s}^{-1}$. The curve for an amorphous silicon sample ($SC = 15\%$) is shown for reference. For an i-layer prepared at $SC = 6.25\%$ ($I_{CRS} \approx 4\%$), a distinct ‘S’

shape can no longer be discerned, nor is a peak in dJ_p/dV visible. The photogating signal (not shown here) does however exhibit a distinct peak at low bias, with QE rising to 30 at 2 V. Thus, correspondence between photogating and dJ_p/dV is not exact, although observations suggest this is restricted to cases where the QE peak occurs at low reverse bias. In order to simulate this behaviour correctly, a lower model defect density is required, suggesting that the i-layer is less defective than for fully amorphous material, contrary to spin density studies [11]. However, under AM1.5 conditions the low-crystalline cell performs poorly compared with the amorphous cell, yielding an efficiency of some 2.5% compared with 5% [5].

Reduction of SC to 6% further increases the crystallinity, to approximately 25%. The initial rise of photocurrent with reverse voltage is now much steeper, although the curve flattens off below the saturation current and then increases in a similar way to the $SC = 5.5\%$ cell. It is evident that charge extraction from the generation region is not impeded to the same extent by space-charge limitations as in amorphous silicon, although there is still significant recombination loss overall.

At $SC = 5.5\%$, the i-layer crystallinity is over 60%. The short-circuit current is some 90% of the current extracted at 20 V reverse bias, which indicates that recombination loss is low even under high generation rate conditions in a rather thick cell. A photovoltaic efficiency of 8.5%, typical of a good cell, was obtained under standard AM1.5 test.

The disappearance of space-charge limited features with increasing i-layer crystallinity is consistent with increasing TOF hole mobility reported previously [3-5]. We also obtain qualitative agreement from computer modelling, by varying the hole band mobility between 0.1 and 10 $\text{cm}^2/(\text{Vs})$. This lends support to the work of Liang *et al.* [12], who propose that space-charge trapped in the valence band tail limits amorphous silicon solar cell efficiency.

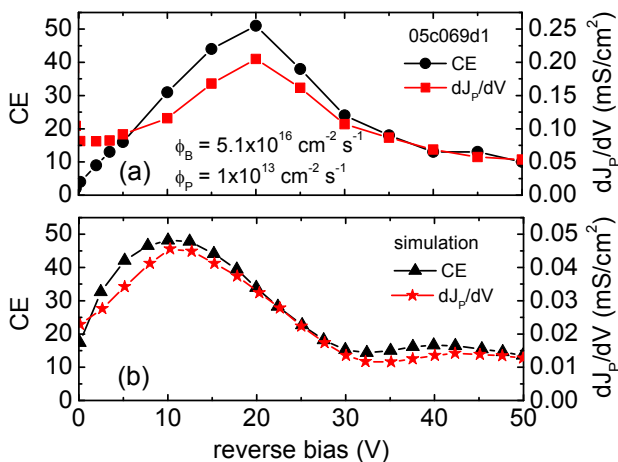


Figure 3 (a) Collection efficiency CE and derivative of photocurrent dI_p/dV vs. reverse bias. (b) computer simulation, using parameters appropriate for light-soaked amorphous silicon.

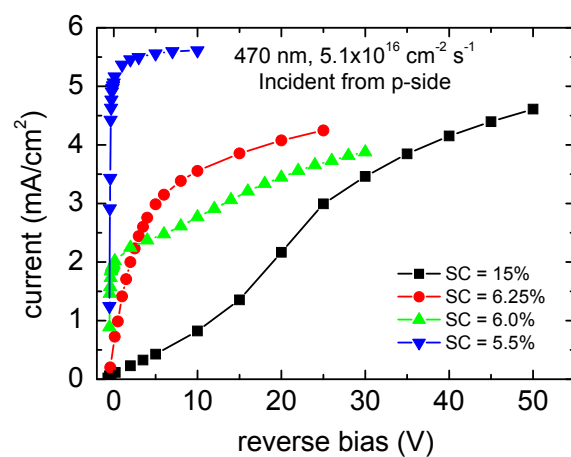


Figure 4 Photocurrent vs. reverse bias (high flux) for samples prepared over a range of SC . Blue light is incident from the p-side.

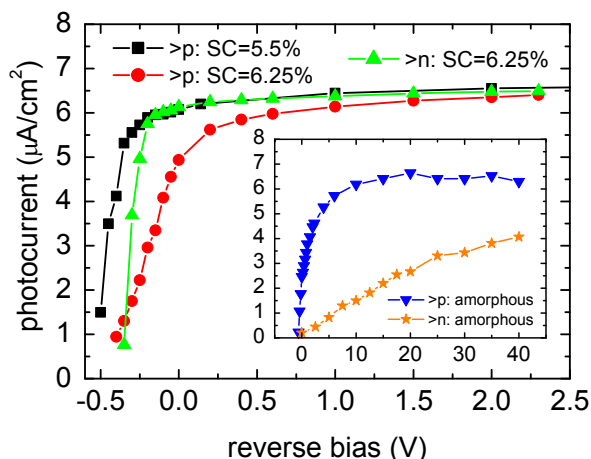


Figure 5 Photocurrent vs. reverse bias voltage for samples prepared over a range of SC, at a 470 nm flux of $5.1 \times 10^{13} \text{ cm}^{-2} \text{ s}^{-1}$ incident from p- or n- side (denoted >p and >n respectively).

3.4 Low generation rate conditions Figure 5 shows photocurrent vs. reverse bias curves measured at reduced 470 nm flux, under either p- or n-side illumination. Features associated with space-charge limitation are absent, and the curves follow the form given by Eq. (2). For p-side illumination by strongly-absorbed light, the *electron* primary photocurrent might be expected to contribute a greater proportion of the terminal current. If so, then full electron collection is more readily achieved (*i.e.* at a lower reverse bias) in the microcrystalline cells, even with a crystalline volume fraction of only 4%, than in the amorphous cell. Similarly, for n-side illumination *hole* transport limits the terminal current, and the contrast between the amorphous and the microcrystalline cells is even more striking. This is in keeping with the increased hole mobility measured in microcrystalline cells using TOF [5]. The TOF work also hints at a *reduction* in electron mobility in low-crystallinity cells, below that in amorphous silicon, but this is not evident in the results presented here. Based solely on the low-excitation results, we might anticipate the amorphous cell (SC = 15%) would be the least-efficient under AM1.5 test conditions, when in fact the poorest performer is the cell prepared at SC = 6.25%, with a crystalline volume fraction of 4%. The reasons for this remain unclear, and further investigations are planned.

4 Conclusions Strongly-absorbed light of flux exceeding $10^{15} \text{ cm}^{-2} \text{ s}^{-1}$ incident on the p-side of thick amorphous silicon pin structures results in a strongly nonlinear photocurrent-flux response. This is consistent with formation of space charge close to the p-i interface, which dominates transport by lowering the local electric field. The ‘S’ shape inflection in the photocurrent-reverse bias curve, and resulting peak in its derivative, occur as the field restriction is overcome and the electron drift current out of the space-charge region becomes limited by the optical generation rate. Computer simulations confirm that similar conditions

are responsible for the photogating effect, in which the p-i space-charge is strongly modulated by holes generated by a weakly absorbed light source becoming trapped in the bulk of the i-layer. This behaviour changes considerably as the crystalline content of the i-layer is increased. Photogating may still be seen in low-crystallinity devices, though the peak is shifted to lower reverse bias, as predicted if the defect density is reduced, or alternatively, if the hole mobility is increased in accordance with time-of-flight measurements. This implies that photogating experiments should not necessarily be interpreted solely in terms of deep defect density. In more highly crystalline devices where good AM1.5 solar cell performance is achieved, little or no evidence of space-charge limitation is seen. Measurements under low optical flux from the n-side reveal a striking difference in extraction behaviour between amorphous and low-crystalline ($I_{CRS} < 5\%$) cells, consistent with an increase of 1 to 2 orders of magnitude in hole mobility-lifetime product. Under p-side illumination, there is no clear support for the low electron mobilities in this deposition regime reported recently for time-of-flight.

Acknowledgements We are grateful to Yaohua Mai and Aad Gordijn for sample preparation, Markus Hülsbeck for Raman measurements, and thank Reinhard Carius for his advice.

References

- [1] A. V. Shah, H. Schade, M. Vanecek, J. Meier, E. Vallat-Sauvain, and N. Wyrsh, *Prog. Photovolt: Res. Appl.* **12**, 113 (2004).
- [2] C. Smit, R. A. C. M. M. van Swaaij, H. Donker, A. M. H. N. Petit, W. M. M. Kessels, and M. C. M. van de Sanden, *J. Appl. Phys.* **94**, 3582 (2003).
- [3] T. Dylla, F. Finger, and E. A. Schiff, *Appl. Phys. Lett.* **87**, 032103 (2005).
- [4] T. Dylla, S. Reynolds, R. Carius, and F. Finger, *J. Non-Cryst. Solids* **352**, 1093 (2006).
- [5] S. Reynolds, R. Carius, F. Finger, and V. Smirnov, *Thin Solid Films* **517**, 6392 (2009).
- [6] C. Main, J.-H. Zollondz, S. Reynolds, W. Gao, R. Brüggemann, and M. J. Rose, *J. Appl. Phys.* **85**, 296 (1999).
- [7] H. Li, F. Rubinelli, J. Rath, and R. E. I. Schropp, 21st European Photovoltaic Solar Energy Conference, Dresden, Germany, 4 - 8 Sept. 2006.
- [8] C.-D. Abel, H. R. Pais, and G. H. Bauer, *Mater. Res. Soc. Symp. Proc.* **219**, 851 (1991).
- [9] Y. Mai, S. Klein, R. Carius, J. Wolff, A. Lambertz, and F. Finger, *J. Appl. Phys.* **97**, 114913 (2005).
- [10] A. M. Meftah, A. F. Meftah, and A. Merazga, *J. Phys.: Condens. Matter* **18**, 5459 (2006).
- [11] F. Finger, L. B. Neto, R. Carius, T. Dylla, and S. Klein, *Phys. Status Solidi C* **1**, 1248 (2004).
- [12] J. Liang, E. A. Schiff, S. Guha, B. Yan, and J. Yang, *Appl. Phys. Lett.* **88**, 063512 (2006).